Optical Engineering

SPIEDigitalLibrary.org/oe

Rare-earth-doped fiber designs for superluminescent sources

Grethell G. Pérez-Sánchez
Indayara Bertoldi-Martins
Philippe Gallion
Jose A. Alvarez-Chávez

Rare-earth-doped fiber designs for superluminescent sources

Grethell G. Pérez-Sánchez
Centro de Investigación e Innovación Tecnológica del IPN
Cerrada Cecati S/N. Col. Santa Catarina
C.P. 02250, México D. F. MEXICO

Indayara Bertoldi-Martins
Philippe Gallion
Ecole Nationale Supérieure des Télécommunications
TELECOM ParisTech, CNRS
LTCI Paris 75013, France

Jose A. Alvarez-Chávez
Centro de Investigación e Innovación Tecnológica del IPN
Cerrada Cecati S/N. Col. Santa Catarina
C.P. 02250, México D. F. MEXICO
E-mail: jalvarezch@ipn.mx

Abstract. The use of rare-earth-doped fiber section working in amplified spontaneous emission regime for different emission wavelengths is analyzed theoretically. From simulation results, the design of all-fiber superluminescent sources employing different rare earths as dopants for new optical windows and different applications is proposed. Results on different pump and signal powers in forward and backward propagation direction with respect to fiber length are presented. [DOI: 10.1117/1.OE.52.8.086110]

Subject terms: amplified spontaneous emission sources; rare-earth-doped fibers; superluminescent fiber sources; Er^{3+}-; Nd^{3+}; Tm^{3+}-; Er^{3+}/Yb^{3+}-; Tm^{3+}/Yb^{3+}–doped amplified spontaneous emission fiber sources.

Paper 130711P received May 17, 2013; revised manuscript received Jul. 2, 2013; accepted for publication Jul. 9, 2013; published online Aug. 21, 2013.

1 Introduction

Over the last few years, fiber-device technology has reached a mature status and is continuing to evolve. Although amplified spontaneous emission (ASE) is considered sometimes a detrimental component in all-fiber devices, in applications such as fiber gyroscopes and broadband sources for the 1550 nm Telecomm window, it is convenient for generating long wavelengths with no longitudinal mode structure and high power with short coherence lengths. Furthermore, broadband diode pumped fiber amplifiers with >30-dB gain have been achieved.[1] Kilowatt-class single-frequency fiber sources have been a dot in the dramatic development curve of these devices. As for broadband devices and their wide tuning capacity, multimode interference effects,[2] optical fiber fattening,[3] and even laser tuning from 1530 to 1602 nm was reached with an Er^{3+}/Yb^{3+} source.[4] Just recently, all-fiber superluminescent sources have become an option for various sensing and Telecomm applications due to their thermal stability, wide spectrum at their output, and their relatively high power handling capacity even at the prototype stage.[5] In this direction, all-fiber lasers and amplifiers doped with rare earths (REs) have contributed to the fast development of long-haul communication systems. In optical transport networks, for instance, one of the latest network developments, the so-called dense wavelength division multiplexing (DWDM) has attracted great interest for long-haul and ultra-long-haul reach due to the fact that RE fiber optic amplifiers and Raman amplifiers are available to amplify the wavelengths transmitted along the network without requiring an optoelectrical signal conversion.[6]

From the design point of view, the resulting output spectrum of an ASE source is determined by different design parameters such as absorption and emission cross-section of the RE-dopant σ_{abs}, σ_{em}, total doping concentration N_T, core radius a, fiber length L, energy level lifetime τ, absorption and emission wavelength σ_{abs}, σ_{em}, and coupled power P_{in}. For these purposes, it would indeed be difficult to change certain proprietary design parameters in commercially available fibers. Consequently, in this work, we propose to only make use of easy-to-modify design parameters, such as fiber length and coupled power, in order to explore ASE conversion efficiency and output spectrum both in forward and backward propagation, based on our recent work but extending it into other REs.

In order to explore the best results from different RE-doped ASE sources, different input powers were used in the modeling. In our simulations, it has been observed that in some cases the lifetime of some energy levels proved to be too short, and in combination with Einstein's $A = 1/\tau$ coefficient, it makes an impact by limiting the total ASE level, which causes laser generation to appear just after very short lengths of fiber. Such limiting behavior could have been prevented by using another host during the fabrication of the studied fibers. The highest-obtained efficiencies for the set of REs used are shown, after variations of fiber length and coupled pump power.

In this piece of work, we present a comparison between Er^{3+}, Nd^{3+}, Pr^{3+}, Tm^{3+}, Tm^{3+}/Yb^{3+}, and Er^{3+}/Yb^{3+} broadband sources based on the same variables of design, with all of them being considered as superluminescent sources in the different optical communications windows. For this study, some specific atomic-level processes have to be considered, as explained below.

For Er^{3+}-doped ASE sources, they are especially important due to the fact that their emission spectrum is around 1550 nm, which is coincident with the lowest losses band for silica fiber. Nevertheless, erbium multilevel energy structure limits its quantum efficiency required for other 1550 nm applications.[7] On the other hand, a codoping technique where Yb^{3+} acts as a sensitizer for Er^{3+} molecules contained

in the lattice, the Yb^{3+} ions in their excited level $^2F_{5/2}$, allow the energetic transfer to the Er^{3+} ions in the exited level $^4I_{11/2}$, via energetic cooperation. Thus having a nonradiative decay to the lower level $^4I_{13/2}$, and finally falling radiatively to the ground level $^4I_{15/2}$ (see Fig. 1). Therefore, giving the system another way for pumping. This system has an improvement in output power around 1550 nm due to this process of sensitizing between both REs with a typical concentration ratio of 10:1, being 10 for ytterbium and 1 for erbium.[8–10]

As for thulium-doped ASE sources at 2 μm, due to the high demand for capacity of WDM systems, the development of such devices at a new transmission window will soon be required. Tm^{3+} is promising in optical communications systems as it is possible to pump Tm^{3+} at 790 nm, where efficient, not-so-expensive laser diodes are available. Furthermore, among the other REs, Tm^{3+} has the widest emission band around 1.8 to 2.1 μm.[11,12] In addition, an alternative to increase the efficiency emission from Tm^{3+} around 2 μm is to codope Tm^{3+} with Yb^{3+} and pump it from 910 to 980 nm. From the so-called cross-relaxation process, efficient 2 μm source operation can be achieved by using the $^3F_4 - {}^3H_6$ pump transition. Tm^{3+} has its level $^3H_5$, which is quasiresonant coincident with the excited Yb^{3+} level $^2F_{5/2}$. As already mentioned, Yb^{3+} has the advantage of possessing only two multiplets: the ground-state level $^2F_{7/2}$ and the excited-state level $^2F_{5/2}$, resulting in a highly efficient absorption from 900 nm to 1 μm. This particular energy level structure is highly desirable for an efficient absorption using commercially available laser diodes that emit 980 nm energy, in order to allow sensitization of Tm^{3+}-doped fibers with Yb^{3+}, as shown in Fig. 2.

All fiber ASE Nd^{3+}- and Pr^{3+}-doped ASE sources are also modeled in this work since such devices could be used in the second Telecomm window at 1310 nm. Direct $^3H_4 - {}^1G_4$ pumping could be used in Pr^{3+}-doped fibers with commercial titanium–sapphire laser at 1005 nm; the optimum absorption wavelength in this transition is at 1038 nm. The emission around 1310 nm is generated in the $^1G_4 - {}^3H_5$ transition.[13,14] Here we also propose an alternative around this window. We propose Nd^{3+} doping. The absorption is at 800 nm in order to obtain the desired emission. The 1310-nm emission is due to the $^4F_{3/2} - {}^4I_{13/2}$ transition.[15,16]

ASE thulium sources can have applications within the S optical communications window at 1470 nm. Using the $^3F_4 - {}^3H_4$ pump transition at 800 nm (Refs. 17 and 18),

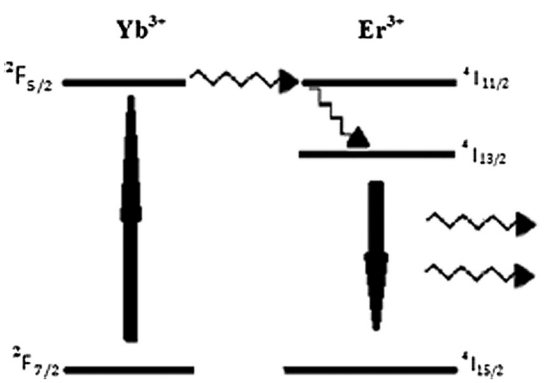

Fig. 1 Er^{3+}/Yb^{3+} energetic transfer process.

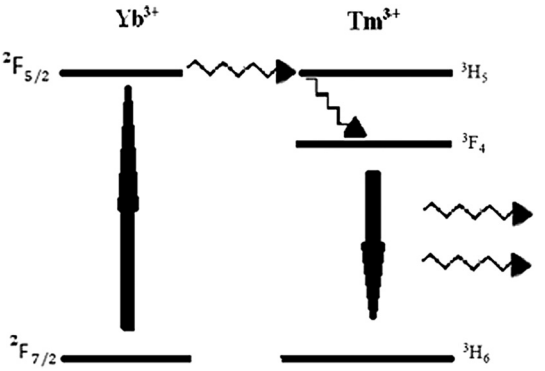

Fig. 2 Tm^{3+}/Yb^{3+} energetic transfer process.

where commercial pump diodes are available, the emission around 1470 nm is generated in the $^3F_4 - {}^3H_6$ transition.

All RE transitions with different single dopants and codoping schemes are theoretically studied by using a simple model, explained in the following sections.

2 Theoretical Model

We used a modified version of rate equations model for three-state laser source considered in ASE regime.[19,20] In this paper, the model is based on a modified version of the aforementioned Einstein rate equations, whose solution allows us to describe the evolution of pump and signal powers, for fixed pump power level and optimal fiber length and maximized output power.

$$\frac{dP_p(Z)}{dz} = -\gamma_p(Z)P_p(z), \tag{1}$$

$$\frac{dP_s^{\pm}(z,\lambda_i)}{dz} = \pm\{G_e(z,\lambda_i)[P_s^{\pm}(z,\lambda_i) + P_0] - G_a(z,\lambda_1)P_s^{\pm}(z,\lambda_1)\}, \tag{2}$$

where $P_p(z)$ is the pump power propagating in z direction parallel to the doped optical fiber axis, $P_s^{\pm}(z,\lambda_1)$ is the output power in forward and backward directions, $\gamma_p(z)$ is the absorption coefficient, $G_e(z,\lambda_1)$ is the amplification of spontaneous emission, $G_a(z,\lambda_1)$ is the absorption coefficient of spontaneous emission, and P_0 represents an equivalent input noise power.

$$P_0 = 2hv_s\Delta s, \tag{3}$$

$$\Delta s = \left(\frac{c}{\lambda_s^2}\right)\Delta\lambda_s. \tag{4}$$

This analysis is performed in weak signal regime for $P_s < P_{\text{sat}}$ and by assuming

$$\gamma_p(z) = \frac{N_T\sigma_p}{\frac{P_p(z)}{P_p^{\text{th}}}+1}, \tag{5}$$

when $P_p(z) < P_p^{\text{th}}$, where P_p^{th} is the threshold power.

$$P_p^{\text{th}} = \pi a^2 \frac{h\nu_p}{\sigma_p \tau}, \tag{6}$$

when $P_p(z) > P_p^{\text{th}}$ From Ref. 21, we consider Eq. (1) as

$$\frac{\mathrm{d}P_p(z)}{\mathrm{d}z} = -N_T \pi a^2 \frac{h\nu_p}{\tau}. \tag{7}$$

Solving Eq. (7) with boundary conditions, $P_p(0) = P_{\text{in}}$, where P_{in} is the initial pump (coupled) power and is described by

$$P_p(z) = P_{\text{in}} - \left(N_T \pi a^2 \frac{h\nu_p}{\tau}\right) z. \tag{8}$$

From Eq. (2) and by considering again weak operation and under the conditions $P_s^+(z=0,\lambda_i) = 0$ and $P_s^-(z = L,\lambda_i) = 0$,

$$G_e(z,\lambda_i) = \frac{N_T \sigma_e(\lambda_i)(1-\eta)\left(\frac{P_p(z)^{\text{th}}}{P_p}\right)}{\frac{P_p(z)^{\text{th}}}{P_p} + 1}, \tag{9}$$

$$G_a(z,\lambda_i) = \frac{N_T \sigma_a(\lambda_i)(1-\eta)1}{\frac{P_p(z)^{\text{th}}}{P_p} + 1}, \tag{10}$$

$$G_b(z,\lambda_i) = G_e(z,\lambda_i) - G_a(z,\lambda_1). \tag{11}$$

The overlap factor for ASE propagation in a single-mode fiber both doped and undoped does depend on wavelength and mode field diameter. This dependency has been accepted as being a ratio similar to core-to-cladding geometrical ratio. In our case, the overlap factor is described by the following equation, which depends on the fiber core radius a and the power mode spot size ω_s on the signal wavelength. This overlap factor is taken into account in G_e and G_a. Γ is the overlap expressed as

$$\Gamma = \exp\left(\frac{-a^2}{\omega_s^2}\right). \tag{12}$$

We therefore obtain

$$P_s^+(z,\lambda_i) = \left(\frac{G_e(z,\lambda_i)}{G_b(z,\lambda_i)} P_0 e^{zG_b(z,\lambda_i)} - \frac{G_e(z,\lambda_1)}{G_b(z,\lambda_1)}\right) \tag{13}$$

$$P_s^-(z,\lambda_i) = \left(\frac{G_e(z,\lambda_i)}{G_b(z,\lambda_i)} P_0 e^{(L-z)G_b(z,\lambda_i)} - \frac{G_e(z,\lambda_1)}{G_b(z,\lambda_1)}\right). \tag{14}$$

For the model presented, three differential equations are defined. Such equations determine pump power, copropagating signal power, and also counterpropagating signal power, for different input powers and fiber lengths, on which the pump power wavelength is represented via its corresponding pump frequency, ν_p. Furthermore, in order to determine forward and backward ASE power levels in the model, we only take the peak value where emission is maximum and then we take the corresponding value of λ_i in the spectrum.

In Eq. (15), signal conversion efficiency is defined as output power in terms of the spectral converted signal, divided by the input (coupled) pump power, depending on the active material under study. Now, P_{out} (lambda_converted-signal) is precisely the converted output power of the superluminescent source, resulting from the quantum conversion, whereas P_{in} (lambda_pump-signal) is the amount of pump power at the input point of the superluminescent source at $z = 0$. Finally, in order to calculate the signal conversion efficiency η, we use the following expression:

$$\eta = \frac{P_{\text{out}}(\lambda_{\text{converted-signal}})}{P_{\text{in}}(\lambda_{\text{pump-signal}})}. \tag{15}$$

In the figures shown below, the ASE output for Er^{3+}, Nd^{3+}, Pr^{3+}, Tm^{3+}, Tm^{3+}/Yb^3, and Er^{3+}/Yb^{3+} sources is shown for both counter- and copropagating pump power levels. It has clearly been observed that the ASE efficiency for codoping schemes is normally higher. The results of the different sources are presented in the curves by varying the fiber parameters such as fiber length, input power, and doping RE. We can observe the variation of the pump and output powers in forward propagation direction and backward propagation direction, along the length of the fiber and for different input powers.

For theoretical calculations of pump and signal powers in Figs. 26–35 in the Appendix, we used a total concentration of $N_T = 1.9 \times 10^{25}$ ions/cm^3, core radius of $a = 2$ μm, and an appropriate pump wavelength, according to the absorption cross-section of the RE molecules, as shown in the Appendix.

2.1 Er^{3+} and Er^{3+}/Yb^{3+} ASE at 1550 nm

Amplified spontaneous emission power and gain simulations from Er^{3+} and Er^{3+}/Yb^{3+}-doped fibers are shown in Figs. 3–6 in the region of 1550 nm.

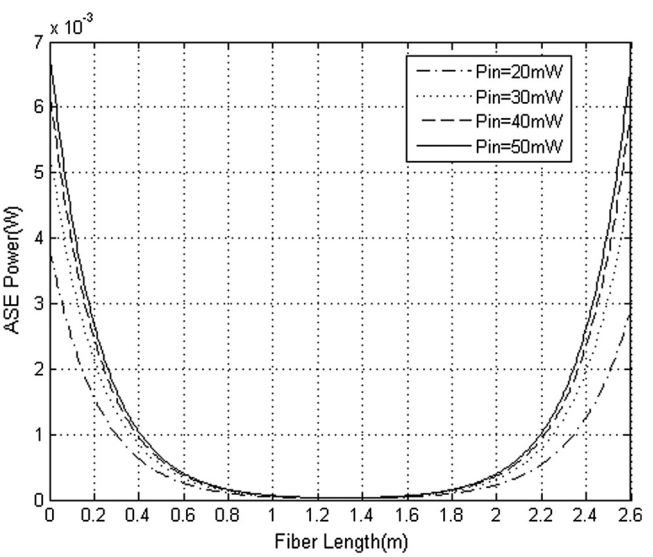

Fig. 3 ASE backward-forward output power versus fiber length with $P_p = 20$, 30, 40, and 50 mW for Er^{3+} fiber.

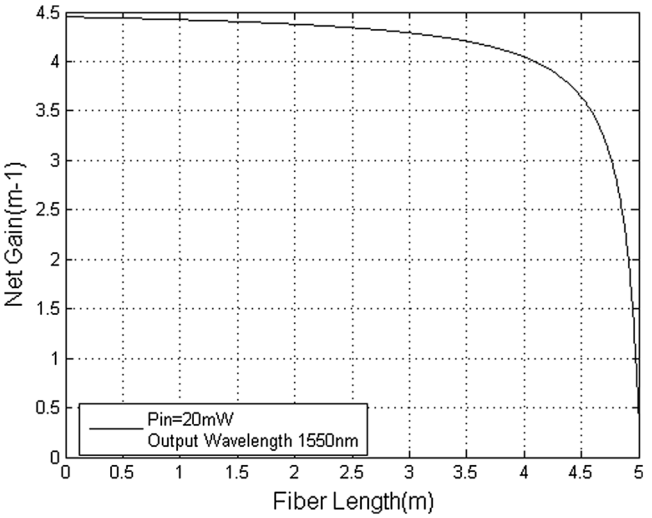

Fig. 4 Net gain versus fiber length with $P_p = 20$ mW. Er^{3+} fiber.

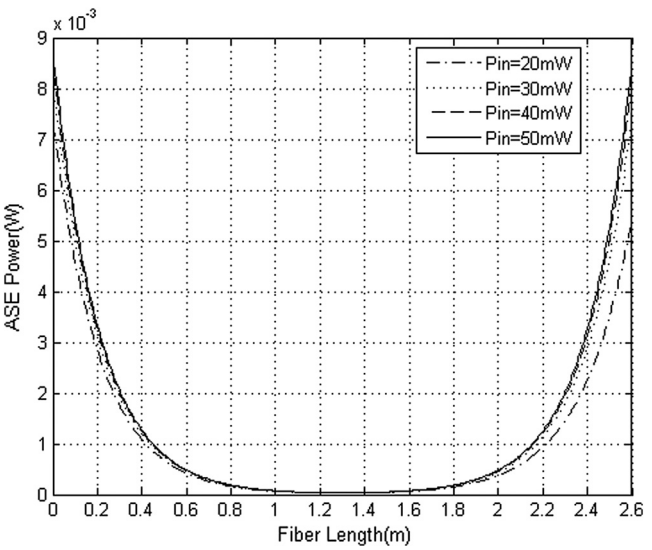

Fig. 5 ASE backward-forward output power versus fiber length with $P_p = 20$, 30, 40, and 50 mW for Er^{3+}/Yb^{3+} fiber.

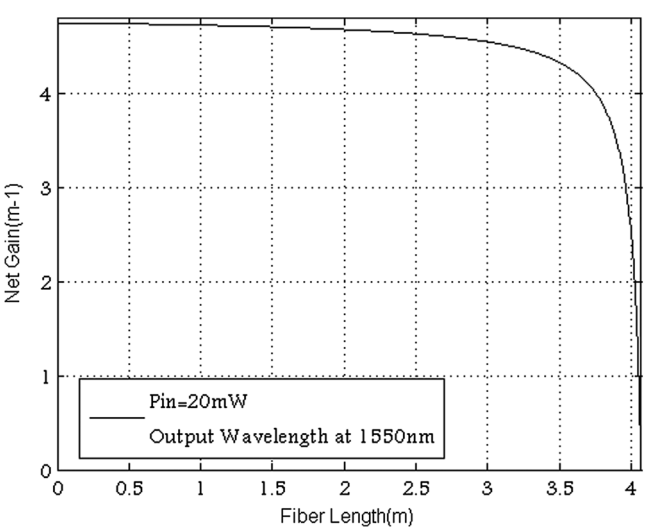

Fig. 6 Net gain versus fiber length with $P_p = 20$ mW. Er^{3+}/Yb^{3+} fiber.

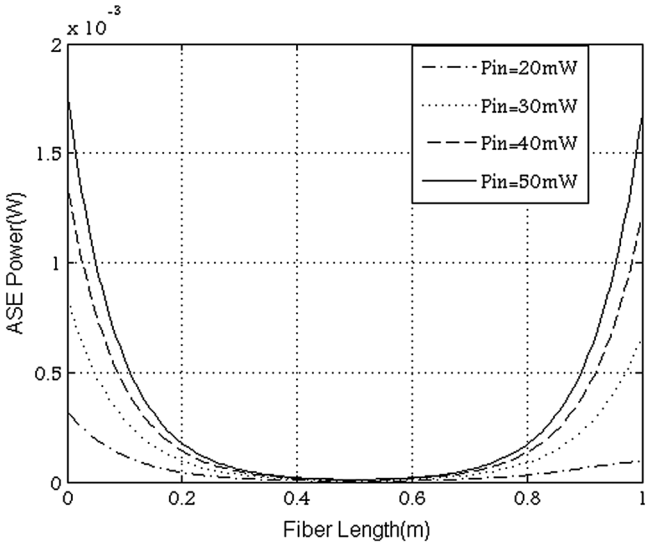

Fig. 7 ASE backward-forward output power versus fiber length with $P_p = 20$, 30, 40, and 50 mW. Tm^{3+} fiber.

2.2 Tm^{3+} ASE at 1900 nm

Note that in Figs. 3, 5, 7–10 ASE backward output power is the ASE power level that propagates in the opposite direction of the pump power. ASE forward output power is the ASE power level that propagates in the same direction of the pump power. We showed the calculated conversion efficiency values, which depend on absorption and emission cross-sections for each active material studied. Also, in Figs. 3, 5, 7–10, we showed the efficiency η_{bw} as the signal conversion efficiency in the opposite direction with respect to the pump. As for η_{fw}, it defines the signal conversion efficiency in the same direction as the pump, i.e., forward.

2.3 Nd^{3+} ASE at 1310 nm

As we can observe in Figs. 11, 12, 13, and 14, the pump power evolution along the fiber shows a declining behavior

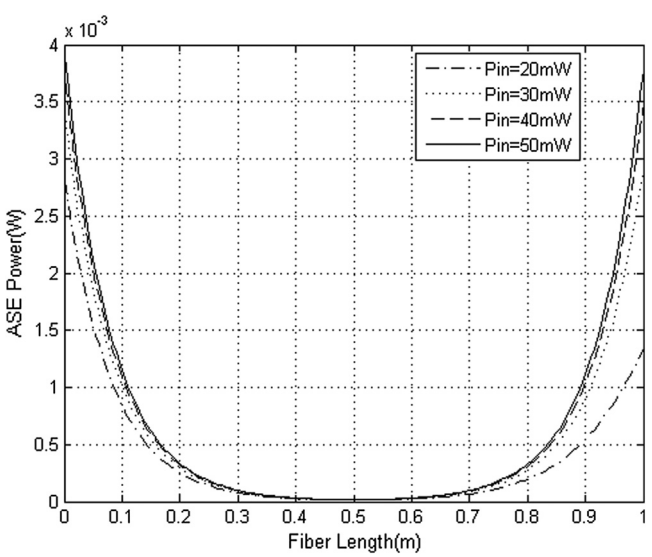

Fig. 8 ASE backward-forward output power versus fiber length with $P_p = 20$, 30, 40, and 50 mW. Tm^{3+}/Yb^{3+} fiber.

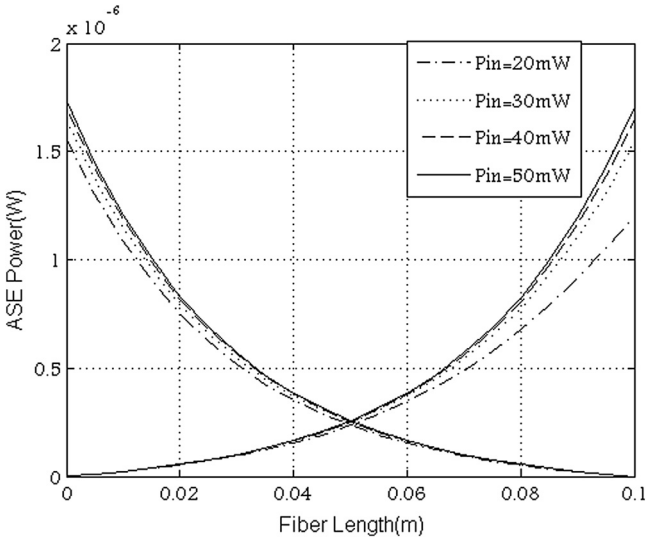

Fig. 9 ASE backward-forward output power versus fiber length with $P_p = 20$, 30, 40, and 50 mW. Nd^{3+} fiber.

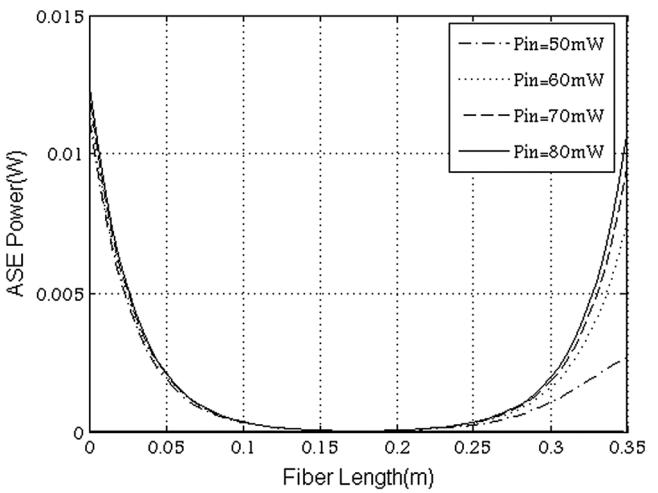

Fig. 10 ASE backward-forward output power versus fiber length with $P_p = 50$, 60, 70, and 80 mW. Nd^{3+} fiber.

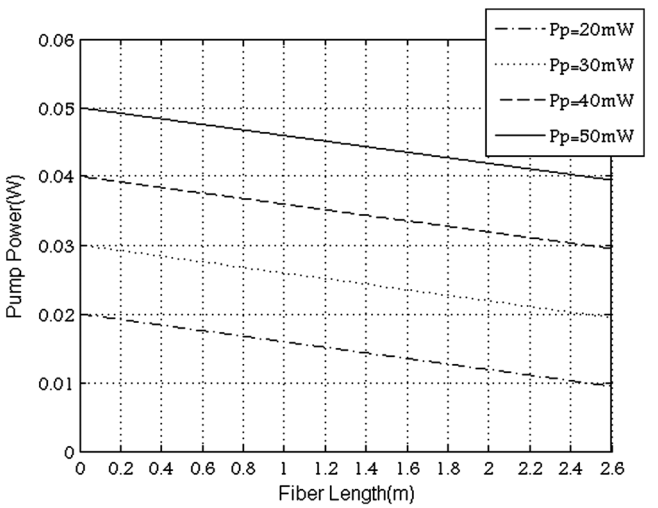

Fig. 11 P_p versus fiber length with $P_p = 20$, 30, 40, and 50 mW for Er^{3+} fiber.

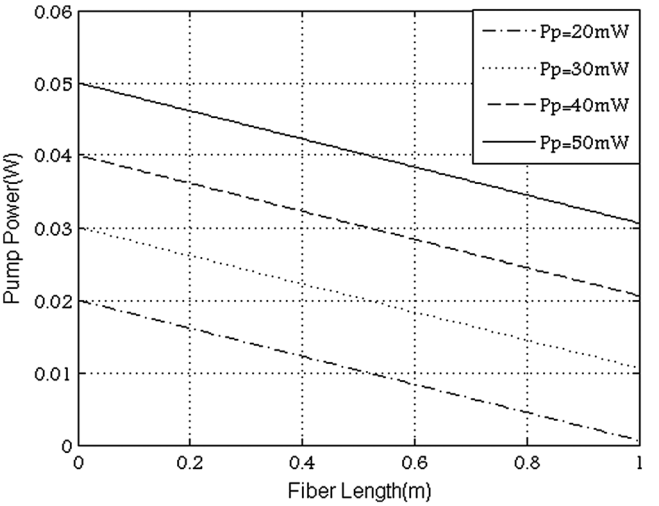

Fig. 12 P_p versus fiber length with $P_p = 20$, 30, 40, and 50 mW. Tm^{3+} fiber.

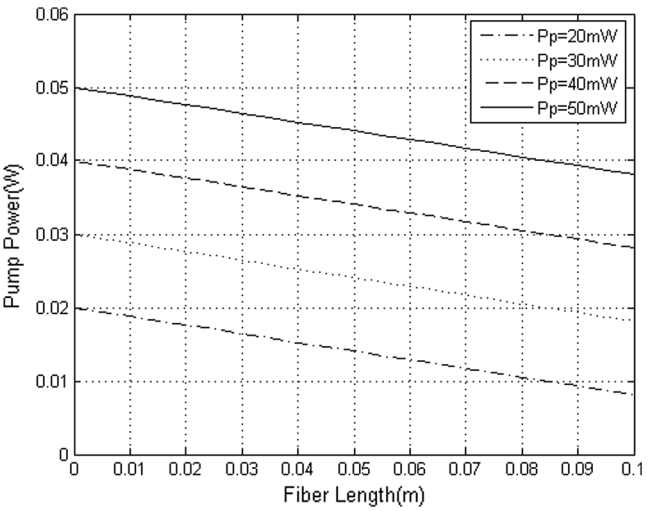

Fig. 13 P_p versus fiber length with $P_p = 20$, 30, 40, and 50 mW. Nd^{3+} fiber.

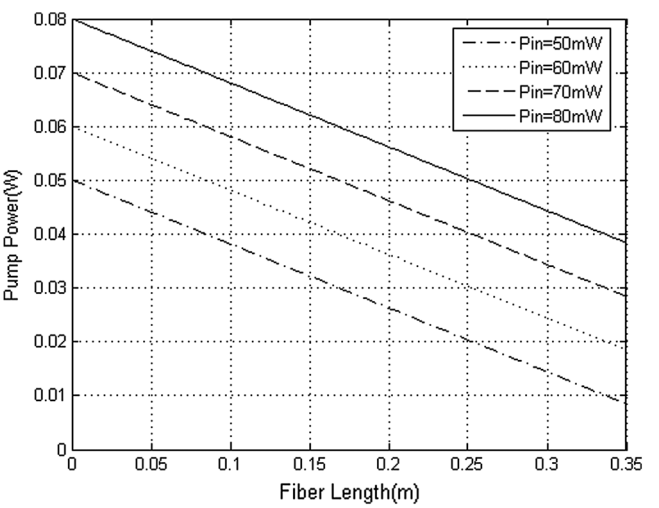

Fig. 14 P_p versus fiber length with $P_p = 50$, 60, 70, and 80 mW. Nd^{3+} fiber.

as background losses and pump energy absorption take place in the pump propagation direction. Absorption cross-section of RE molecules use up the available energy for population inversion and ASE after nonradiative decay from the corresponding excited-state levels, which in turn will allow broadband photon emission. Let us consider that under certain fiber-end circumstances, feedback from Rayleigh backscattering could be sufficient to drive the ASE source above lasing threshold, which would limit ASE power level at the output.

Figures 3, 5, 7–10 represent output power behavior in forward and backward propagation directions along the fiber length for the whole set of REs included in this paper. It can be seen that the backward power is, in general, slightly larger than the forward power due to absorption within the first few sections of the fiber, which generated higher population inversion in those first few fiber sections and which could create an unbalanced ASE source. Figures 15, 16, 17,

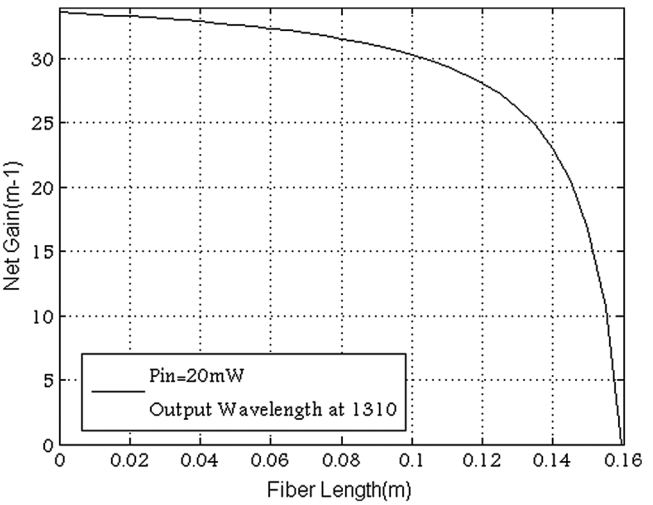

Fig. 17 Net gain versus fiber length with $P_p = 20$ mW. Nd^{+} fiber.

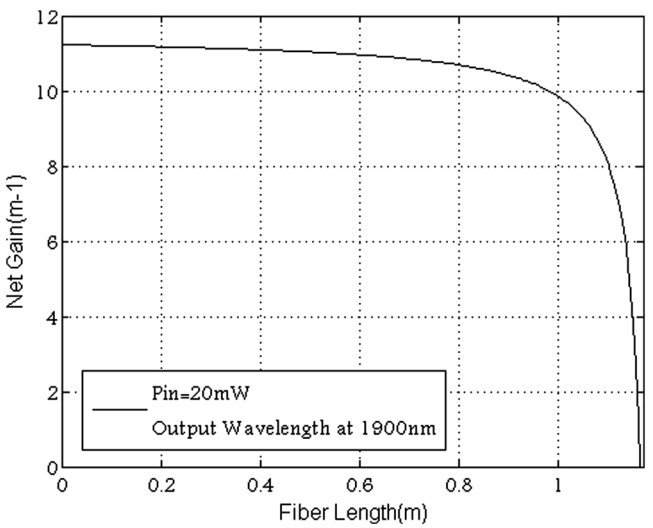

Fig. 15 Net gain versus fiber length with $P_p = 20$ mW. Tm^{3+} fiber.

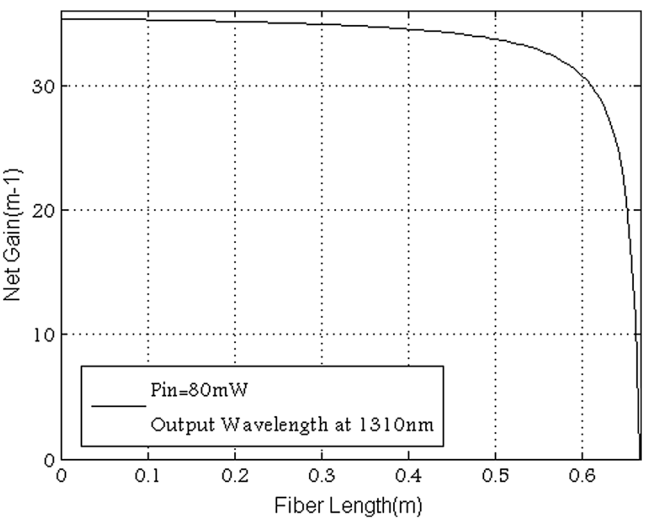

Fig. 18 Net gain versus fiber length with $P_p = 80$ mW. Nd^{3+} fiber.

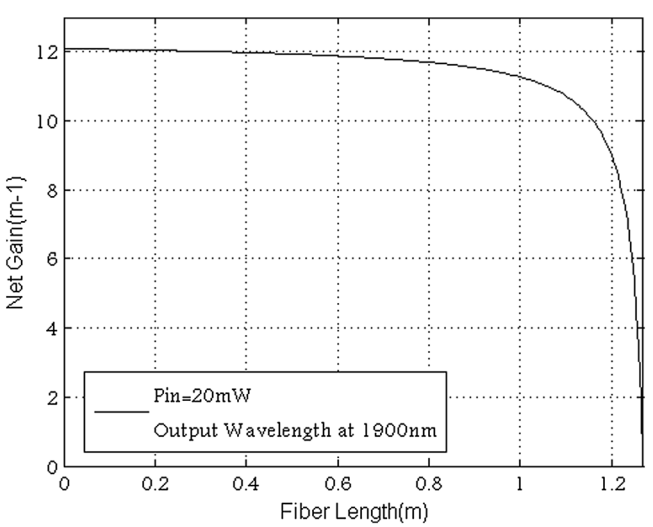

Fig. 16 Net gain versus fiber length with $P_p = 20$ mW. Tm^{3+}/Yb^{3+} fiber.

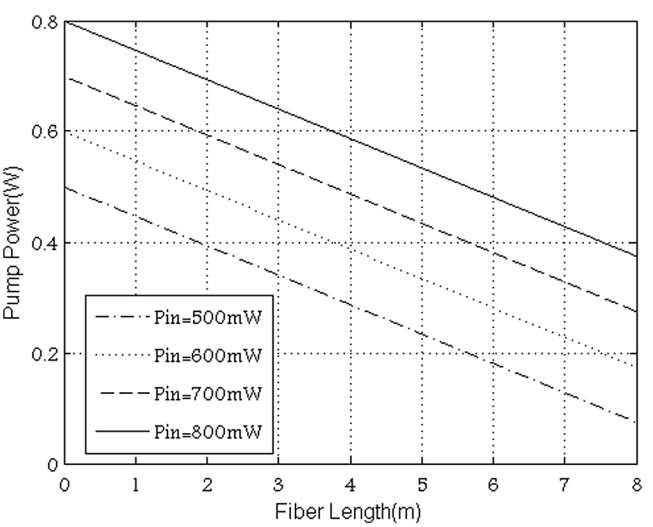

Fig. 19 P_p versus fiber length with $P_p = 500$, 600, 700, and 800 mW. Pr^{3+} fiber.

and 18, represent net gain versus fiber length for Tm^{3+} and Nd^{3+}. Figures 19–21 show pump power, backward and forwards ASE power and net gain, all versus fiber length, for Pr^{3+} sources, respectively.

Some of the applications for 1310 nm ASE sources, such as the ones analyzed in this paper, could include optical component characterization, optical measurement systems, and optical sensing, within the O band. Please note that in early communication systems, the wavelength region situated between 1260 and 1360 nm was called "original band" and that this is the reason it is typically called "O band" as this band is used in different applications such as fiber to the home, among others. In terms of quantum efficiency, for a given fiber length and a given pump power level, the total gain varies along the fiber depending on the absorption and emission Ga and Ge coefficients, which describe the absorption and emission parameters, respectively.[21]

2.4 Tm^{3+} ASE S-band at 1470 nm

As can be observed in Figs. 22 to 25, it has been necessary to increase the input power required for broadband generation and consequently maximum efficiency, which reached up to 58% in the present study.

In Fig. 23, we showed the efficiency η_{bw} as the signal conversion efficiency in the opposite direction with respect to the pump. As for η_{fw}, it defines the signal conversion efficiency in the same direction as the pump, i.e., forward.

2.5 Pr^{3+} ASE O-band at 1310 nm

As expected, the specific design changes due to quantum characteristics natural of each RE.

The lifetime values that were used in this work are listed in Table 1, along with the emission and absorption cross-section values for the different active dopant materials studied in this paper.

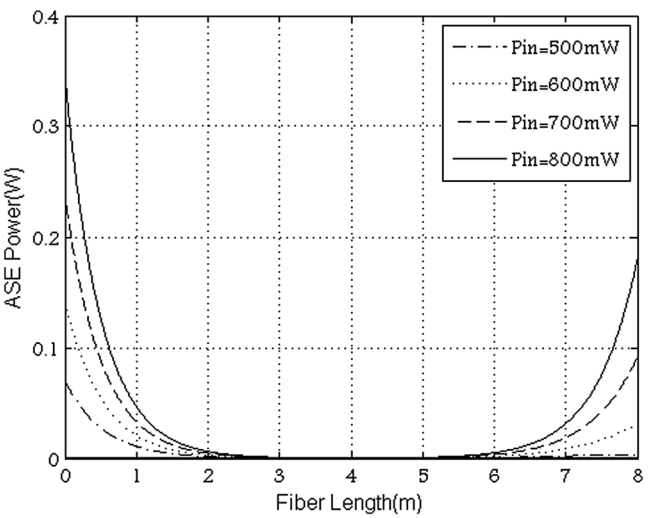

Fig. 20 ASE backward-forward output power versus fiber length with $P_p = 500$, 600, 700, and 800 mW. Pr^{3+} fiber.

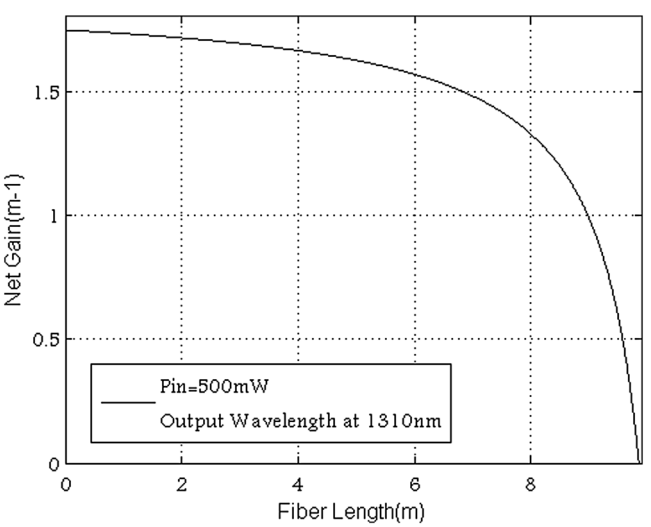

Fig. 21 Net gain versus fiber length with $P_p = 500$ mW. Pr^{3+} fiber.

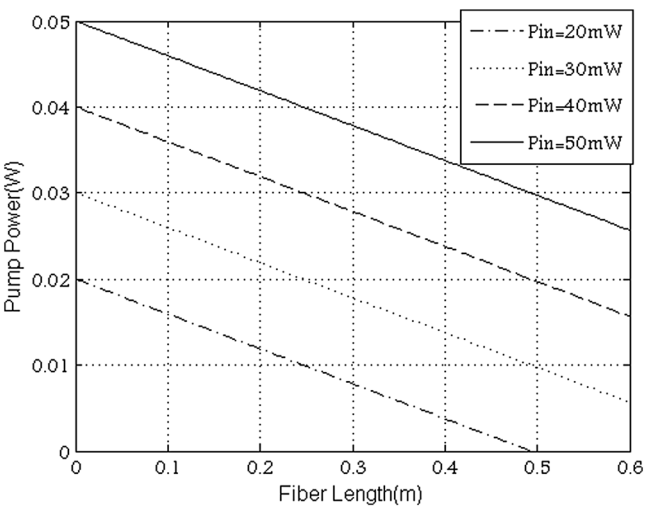

Fig. 22 P_p versus fiber length with $P_p = 20$, 30, 40, and 50 mW. Tm^{3+} fiber.

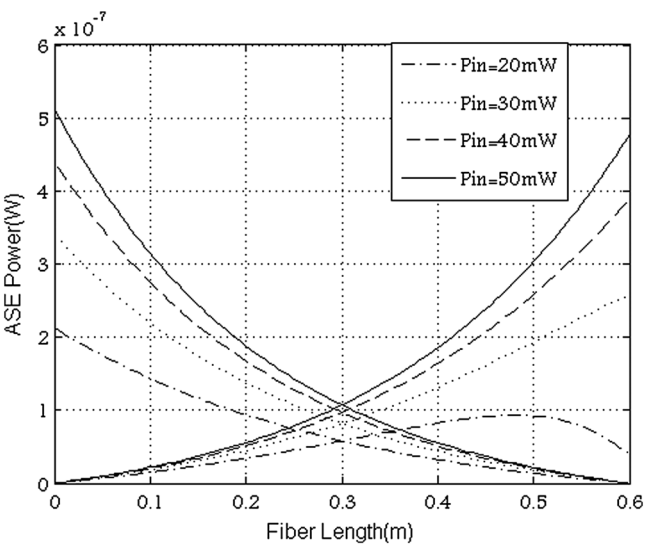

Fig. 23 ASE backward-forward output power versus fiber length with $P_p = 20$, 30, 40, and 50 mW. Tm^{3+} fiber.

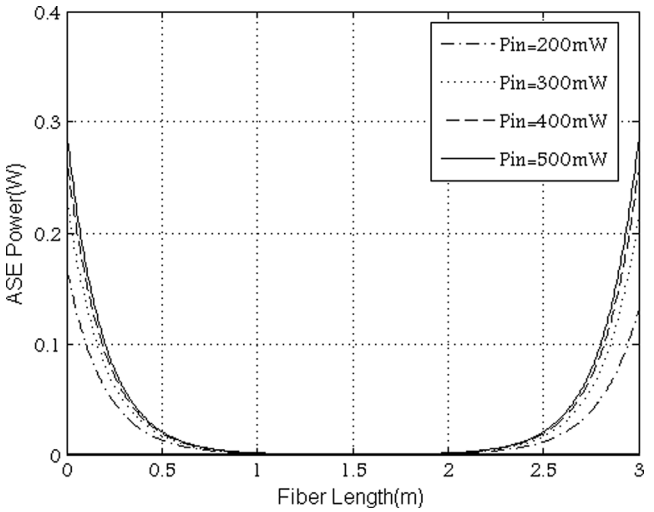

Fig. 24 ASE backward-forward output power versus fiber length with $P_p = 200$, 300, 400, and 500 mW. Tm^{3+} fiber.

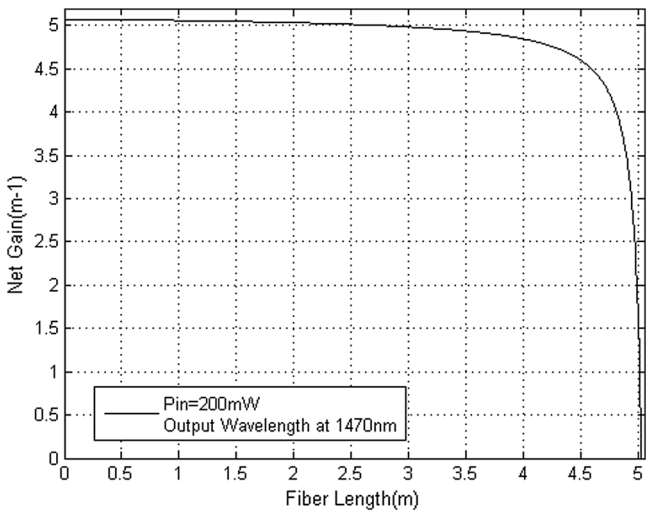

Fig. 25 Net gain versus fiber length with $P_p = 200$ mW. Tm^{3+} fiber.

Moreover, as one can observe in pump propagation and ASE signal figures, each signal with initial pump power $P_p(0)$ reaches a maximum output power; the output power is higher for a higher input power since each pump power level at the fiber input has an ideal fiber length. As expected, we observe that the efficiency increases up to >50% for a codoped scheme ASE with similar simulation parameters of design, both in forward and backward directions compared to a single dopant scheme. The increased output signal in codoped fiber is due to the effective cross-section of Er^{3+} and Tm^{3+} fiber increases via the presence of Yb^{3+} since the total absorption gets higher.

3 Conclusions

Our paper provides simulation results of ASE energy obtained from a series of active RE-doped materials that are being used to develop useful applications in a variety of fields, such as gyroscopes, sensors, and modern Telecommunications in current available optical windows, using a simple modified model based on Einstein's rate equations.

We have shown a generalized, simple method for simulating and obtaining valuable design parameters for superluminescent sources at 1.31, 1.47, 1.55, and even 1.9 μm region and further. This simple method is applied just by modifying the coupled power into the redoped fiber, the fiber length parameter, and as such via the variation of efficiencies for different dopants as shown in the obtained results. Some of the ASE results at 1310 and 1550 nm could be important for communication systems and free-space communication applications. As mentioned before, 1310 nm ASE sources could find applications in optical component characterization, optical measurement systems, and optical sensing in structural health monitoring, for instance. From the codoping results, we can observe the advantage of using a codoped section to increase the output signal power in forward and backward propagating directions, as expected. Our theoretical calculations are useful to explain and even predict the behavior of the superluminescent all-fiber sources in terms of optimum length, total ASE

Table 1 Rare-earth data for the model.

Dopant	Transition	λ_{abs} (nm)	λ_{em} (nm)	Lifetime τ (s)	Absorption cross-section λ_{abs} (m^2)	Emission cross-section λ_{em} (m^2)
Er	$^4I_{13/2} \rightarrow {}^4I_{15/2}$	976	1550	12×10^{-3}	4.839×10^{-25}	8.1×10^{-25}
Er/Yb	$^4I_{13/2} \rightarrow {}^4I_{15/2}$	976	1550	12×10^{-3}	2.5×10^{-24}	8.1×10^{-25}
Nd	$^4F_{3/2} \rightarrow {}^4I_{13/2}$	800	1310	500×10^{-6}	23×10^{-25}	6×10^{-25}
Pr	$^1G_4 \rightarrow {}^3H_5$	1017	1310	879×10^{-6}	0.2×10^{-24}	3.8×10^{-25}
Tm	$^3H_4 \rightarrow {}^3F_4$	790	1470	1.5×10^{-3}	3×10^{-25}	9×10^{-24}
Tm	$^3F_4 \rightarrow {}^3H_6$	780	1900	3.35×10^{-3}	3.3×10^{-25}	2.09×10^{-24}
Tm/Yb	$^3F_4 \rightarrow {}^3H_6$	976	1900	3.35×10^{-3}	2.5×10^{-24}	2.09×10^{-24}

power, gain and conversion efficiency. We can foresee the possibility to use these kinds of fibers to design DWDM sources due to the fact that these kinds of sources have a big spectral broadband.

Finally our results could be used for designing RE-doped superluminescent sources since it predicts output powers and efficiencies in both the forward and backward pump propagation directions. We could venture to recommend our paper for investigating new designs of ASE sources, using a method that modifies the fiber parameters in a simple way, via an optimization route for the desired application.

Appendix: Absorption and Emission Spectra of Studied Rare Earths

The spectra shown (Figs. 26 to 35) were obtained from Refs. 4, 7, 13, and 15.

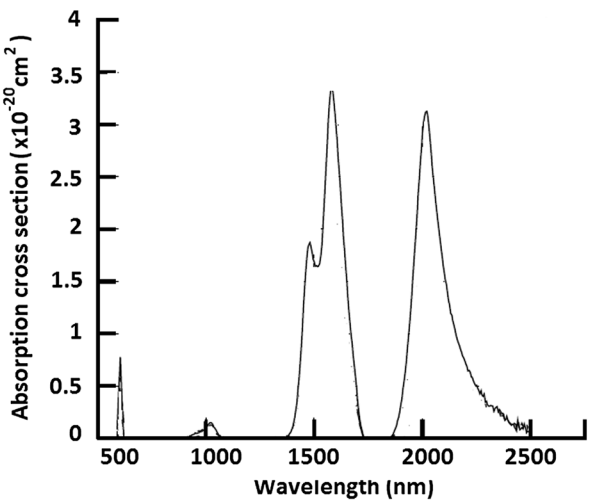

Fig. 26 Absorption cross-section Pr^{3+}.

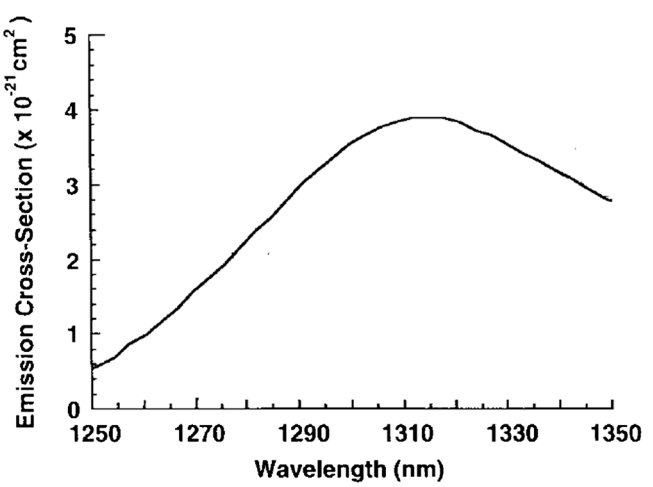

Fig. 27 Emission cross-section Pr^{3+}.

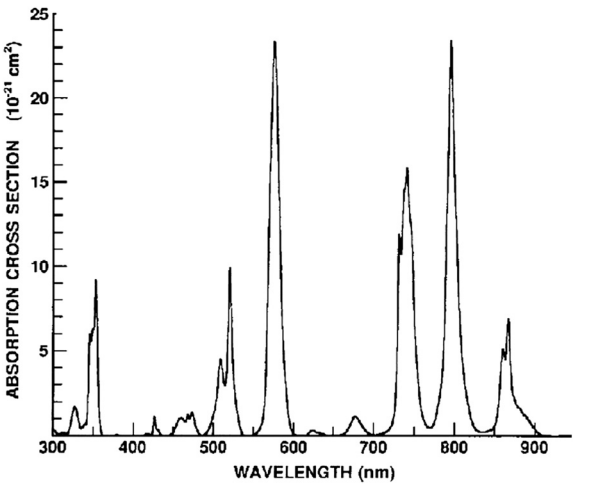

Fig. 28 Absorption cross-section Nd^{3+}.

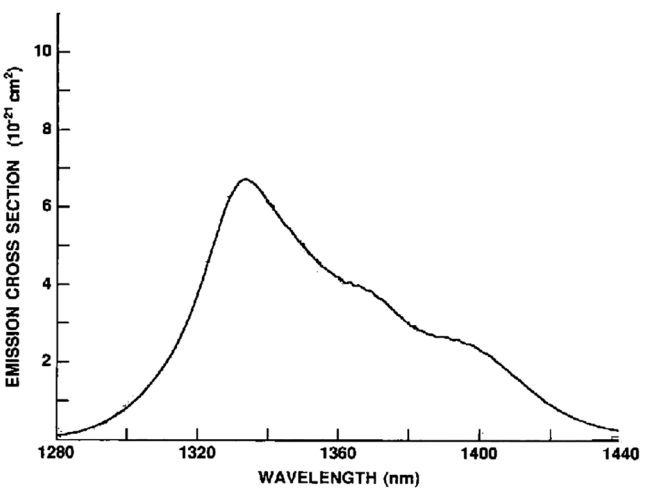

Fig. 29 Emission cross-section Nd^{3+}.

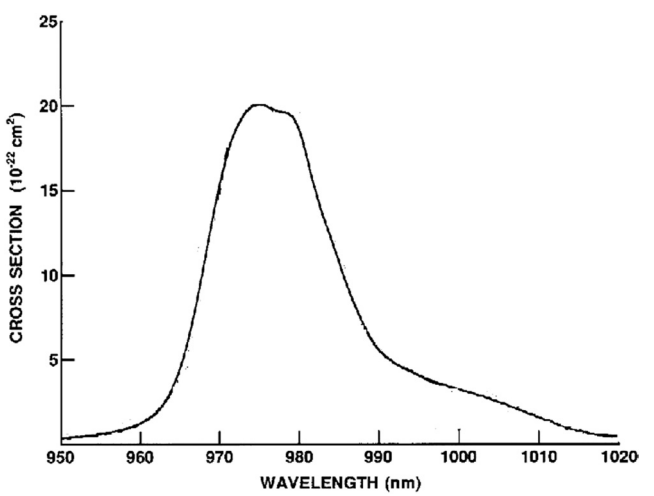

Fig. 30 Absorption cross-section Er^{3+}.

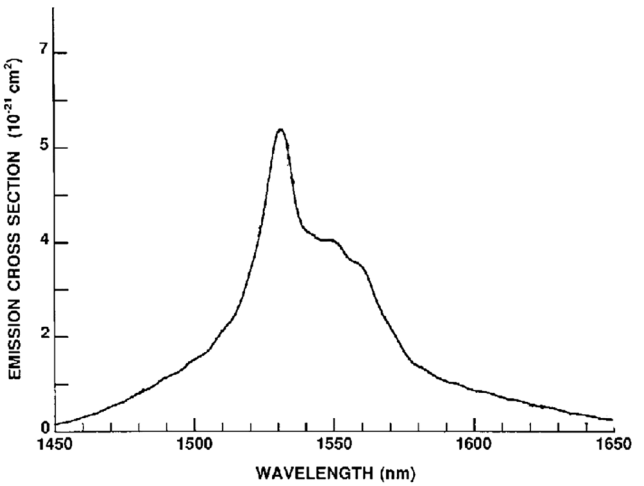

Fig. 31 Emission cross-section Er^{3+}.

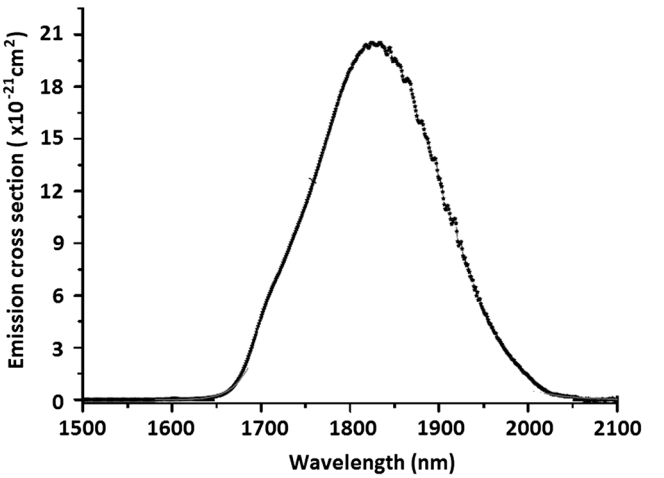

Fig. 34 Emission cross-section Tm^{3+}.

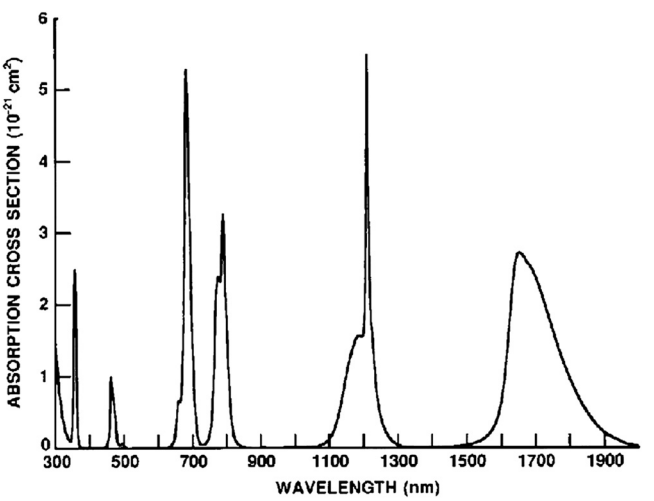

Fig. 32 Absorption cross-section Tm^{3+}.

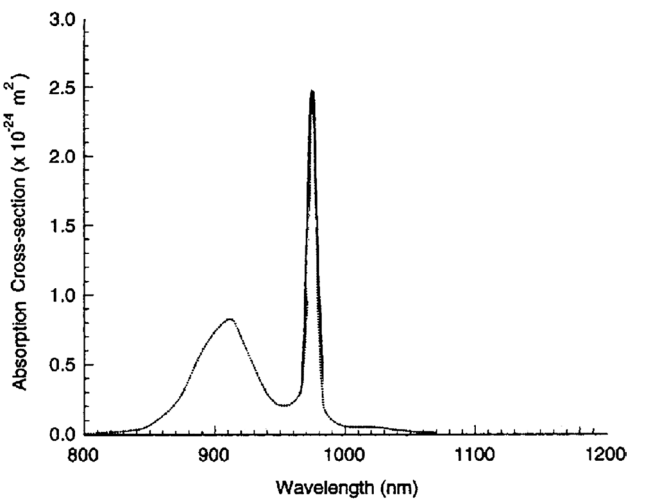

Fig. 35 Absorption cross-section Yb^{3+}.

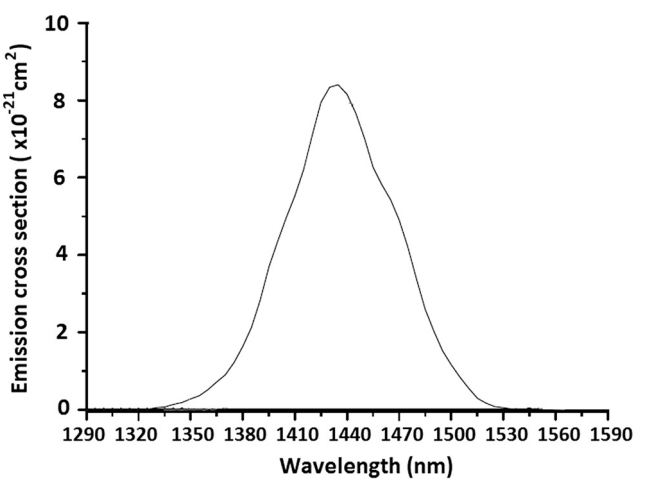

Fig. 33 Absorption cross-section Tm^{3+}.

References

1. J. M. Souza et al., "Broad-band diode-pumped ytterbium-doped fiber amplifier with 34-dBm output power," *IEEE Photon. Technol. Lett.* **11**(1), 39–41 (1999).
2. A. Castillo-Guzman et al., "Widely tuneable erbium-doped fiber laser based on multimode interference effect," *Opt. Express* **18**(2), 591–597 (2010).
3. R. I. Mata-Chávez et al., "Wavelength band-rejection filters based on optical fiber fattening by fusion splicing," *Opt. Laser Technol.* **40**(4), 671–675 (2008).
4. J. Nilsson et al., "High-power and tunable operation of erbium-ytterbium co-doped cladding-pumped fiber lasers," *IEEE J. Quantum Electron.* **39**(8), 987–994 (2003).
5. G. G. Perez-Sanchez, E. Pinzon-Escobar, and J. A. Alvarez-Chavez, "Superluminiscent Er^{3+}/Yb^{3+}-doped fiber source design for 1550 nm applications," *Proc. SPIE* **8497**, 84970U (2012).
6. L. de La Cruz-May et al., "Raman threshold for nth-order cascade Raman amplification," *Opt. Fiber Technol.* **17**(3), 214–217 (2011).
7. M. J. Digonnet, *Rare-Earth-Doped Fiber Lasers and Amplifiers*, 2nd ed., Marcel Dekker Inc., New York (2001).
8. W. L. Barnes et al., "$Er^{3+} - Yb^{3+}$ and Er^{3+} doped fiber lasers," *J. Lightwave Technol.* **7**(10), 1461–1465 (1989).
9. C. Lester et al., "Modeling of Yb^{3+}-sensitized Er^{3+}-doped silica waveguide amplifiers," *J. Lightwave Technol.* **13**(5), 740–743 (1995).
10. R. Ahmad, M. Rochette, and S. Chatigny, "Spectrally wide, and high-power Er-Yb fiber amplifier for 40 Gb/s telecommunications applications," in *Conf. on Lasers, and Electro-Optics, and Quantum*

Electronics, and Laser Science, pp. 1–2, Optical Society of America, Washington, DC (2010).
11. J. Liu and P. Wang, "High-power broadband thulium-doped all-fiber superfluorescent source at 2 um," *Photon. Technol. Lett.* **25**(3), 242–245 (2013).
12. S. W. Harun et al., "Ytterbium-sensitized thulium-doped fiber laser with a single-mode output operating at 1 900-nm region," *Chin. Opt. Lett.* **10**(10), 101401 (2012).
13. R. C. Schimmel, *Towards More Efficient Praseodymium Doped Fiber Amplifiers for the O-Band*, Universiteit Eindhoven, The Netherlands (2006).
14. Y. Nishida et al., "Development of an efficient praseodymium-doped fiber amplifier," *IEEE J. Quantum Electron.* **34**(8), 1332–1339 (1998).
15. E. Lebrasseura et al., "Optical amplification and laser spectroscopy of neodymium-doped fluoride glass channel waveguides," *J. Alloys Compd.* **275–277**, 716–720 (1998).
16. R. F. Kalman, M. J. F. Digonnet, and P. F. Wysocki, "Modeling of three-level laser superfluorescent fiber sources," *Proc. SPIE* **1373**, 209–222 (1990).
17. P. F. Moulton et al., "Tm-doped fiber lasers: fundamentals and power scaling," *IEEE J. Sel. Topics Quantum Electron.* **15**(1), 85–92 (2009).
18. O. Mahran et al., "Wavelength division multiplexing of yttria-alumina-silica doped with thulium optical fiber amplifiers," *Int. J. Res. Rev. Appl. Sci.* **10**(2), 314–321 (2012).
19. E. Desurvire and J. R. Simpson, "Amplification of spontaneous emission in erbium-doped single mode fiber," *J. Lightwave Technol.* **7**(5), 835–845 (1989).
20. G. E. Sandoval-Romero, V. Argueta-Díaz, and O. Pottiez, "Theoretical results of the analytical and numerical solutions of superluminescent fiber sources," *Phys. Status Solidi C* **6**(S1), S227–S230 (2009).
21. E. F. Pinzón-Escobar et al., "Experimental results of the superluminescent fiber laser sources for fiber optic sensors," *Proc. SPIE* **7839**, 78391R (2010).

Grethell G. Pérez-Sánchez obtained a BEng degree in electronics at Metropolitan Autonomous University, Mexico City, in 2005, an MSc in telecommunications at Escuela Superior de Ingenieria Mecanica y Electrica—Instituto Politecnico Nacional in 2011, and is now pursuing a PhD in all-fiber superluminescent sources at Centro de Invetigacion e Innovacion Tecnologica—Instituto Politecnico Nacional. Her research interests range from active and passive fiber devices for telecom and other applications to semiconductor and fiber amplifiers and nonlinear dynamics. She is a member and cofounder of IPN SPIE student chapter and has presented her work in a few international conferences and meetings.

Indayara Bertoldi-Martins received a bachelor's degree in electrical engineering with emphasis in telecommunications from the Pontifical Catholic University of Campinas in 2004 and an MS degree and PhD from the School of Electrical and Computer Engineering of State University of Campinas in 2007 and 2011. Currently she is postdoctoral in Telecom ParisTech. Her interests are in the field of optical communications such as research related to transport layer and physical layer for the development of future optical network technologies.

Philippe Gallion received his PhD from the University of Reims in 1975 and the Doctorates Science from the University of Montpellier in 1986. His present research topics focus on advanced digital communications systems and networks, quantum communication and quantum cryptography, nonlinearity and noise in Raman distributed optical amplifiers. He is a full professor at Télécom Paris Tech. He is an author of several text books, more than 130 international technical publications, and more than 130 communications and lectures at conferences. He is a member of the Optical Society of America and a senior member of the Institute of Electrical and Electronics Engineers. He is the chairman of the IEEE Photonics Society (formerly Laser and Electro Optics Society) French Chapter. He serves on the editorial board and scientific committee of several technical publications and as a member of program or steering committee of international scientific meeting.

Jose A. Alvarez-Chávez received a BEng degree in mechanics at Universidad Nacional Autonoma de Mexico in 1992, obtained an MSc in telecommunications from Centro de Investigacion Cientifica y de Educacion Superior de Ensenada in 1994, and a PhD in fiber lasers and amplifiers from the Optoelectronics Research Centre, Southampton University in 2003. He worked for TelMex and Iusacell in Mexico and Xtera Communications Inc. in the United States in 2002, and Southampton Photonics Ltd. in the United Kingdom in 2005. His research activities include all-fiber active and passive devices, high-power fiber lasers and amplifiers and fiber sensors. He has been a senior research fellow at Centro de Invetigacion e Innovacion Tecnologica—Instituto Politecnico Nacional since 2007.